

## Neutron density distribution and the halo structure of $^{22}\text{C}$

Manjari Sharma,<sup>1</sup> A. Bhagwat,<sup>2</sup> Z. A. Khan,<sup>1</sup> W. Haider,<sup>1</sup> and Y. K. Gambhir<sup>3,4</sup>

<sup>1</sup>*Department of Physics, Aligarh Muslim University, Aligarh 202 002, India*

<sup>2</sup>*UM-DAE Centre for Excellence in Basic Sciences, Mumbai 400 098, India*

<sup>3</sup>*Department of Physics, I.I.T. Powai, Mumbai 400 076, India*

<sup>4</sup>*Manipal University, Manipal 576104, India*

(Received 10 January 2011; published 28 March 2011)

The recently measured reaction cross sections for the neutron-rich carbon isotopes ( $^{19}\text{C}$ ,  $^{20}\text{C}$ , and  $^{22}\text{C}$ ) on a proton target at 40 A MeV are analyzed using the finite range Glauber model (FRGM) and the microscopic optical potential calculated within the Brueckner-Hartree-Fock formalism (BHF). In FRGM nucleon-nucleon cross sections are used, while in the latter (BHF), Hamada-Johnston, Urbana v-14, and the Argonne v-18 internucleon potentials are employed to calculate the microscopic optical potential. The required nucleon density distributions are calculated within the relativistic mean-field (RMF) framework. To test the halo structure, the extended neutron density distribution for  $^{22}\text{C}$  is also used. The analysis reveals that the BHF results of all three internucleon potentials are very close to each other, and also agree with the corresponding results of the FRGM. Our results, using RMF densities, are in agreement with the experimental data for all isotopes of carbon except  $^{22}\text{C}$ , for which we require extended neutron density distribution, indicating a halo structure.

DOI: [10.1103/PhysRevC.83.031601](https://doi.org/10.1103/PhysRevC.83.031601)

PACS number(s): 24.10.Ht, 21.10.Gv, 25.40.Cm, 27.30.+t

Reactions of unstable neutron-rich nuclei with a proton (hydrogen) target is a field of current interest [1], as in the absence of electron scattering it is the only means to probe the matter and/or neutron distribution of exotic nuclei. A nuclear halo is a structure with dilute matter distribution far beyond the core of the nucleus. One of the most famous halo nuclei is  $^{11}\text{Li}$ , discovered by Tanihata *et al.* [2].

The  $^{22}\text{C}$  nucleus has a Borromean character since  $^{21}\text{C}$  is unstable. Recently, Tanaka *et al.* [1] have measured the reaction cross-section data from the neutron-rich carbon isotopes  $A = 19, 20$ , and  $22$  at 40 A MeV. They have observed a large enhancement of proton reaction cross section  $1338 \pm 274$  mb for  $^{22}\text{C}$  as compared with  $754 \pm 22$  mb for  $^{19}\text{C}$  and  $791 \pm 34$  mb for  $^{20}\text{C}$ . Further, the separation energy for the two valence neutrons ( $S_{2n}$ ) in  $^{22}\text{C}$  is only  $420 \pm 940$  keV [3]. These results are very similar to those for the halo nucleus  $^{11}\text{Li}$ .

This new data on carbon isotopes was analyzed by Tanaka *et al.* [1] using the Glauber model. Although they obtained reasonable agreement (listed in Table I of Ref. [1]) for  $^{19,20}\text{C}$ , the enhancement for  $^{22}\text{C}$  was not reproduced. In order to reproduce this enhancement they had to use an extended neutron density distribution for the two valence neutrons in  $^{22}\text{C}$ , with the core  $^{20}\text{C}$  described by the harmonic oscillator wave functions. The neutron separation energy 210 keV and an adjustable parameter (the critical radius  $r_c$ ) were used to describe the extended neutron distribution. The value of the parameter  $r_c$  (reported to be 5.39 fm) was adjusted to reproduce the enhanced reaction cross section. This leads to the neutron rms (root-mean-squared radius:  $\langle r_n^2 \rangle^{1/2}$ ) of 5.4 fm for  $^{22}\text{C}$ .

In the present work we have analyzed the same data using the Glauber multiple (GM) scattering theory and the microscopic optical potential calculated within the Brueckner-Hartree-Fock formalism (BHF).

Both GM and BHF approaches require nucleon density distributions as an important input. These density distribu-

tions are calculated using the relativistic mean-field (RMF) approach. The RMF calculations [4,5] with a frozen gap approximation using an axially symmetric deformed oscillator basis are carried out. The NL3 [6] Lagrangian parameter set is used. The pairing gaps are obtained by reproducing the pairing energies of the relativistic Hartree-Bogoliubov [5] calculations. The ground-state properties are well reproduced, as expected. Most of the carbon isotopes are found to be deformed. Therefore, the  $L = 0$  multipole part of the deformed density is projected out. These spherical density distributions are used in the present reaction calculation. The resulting charge and matter radii shown in Figs. 1 and 2 clearly agree closely with the corresponding experimental values (wherever available) and those reported earlier by various authors.

At such low projectile energies, the conventional zero-range Glauber model (ZRG) has been modified by including the finite-range effects and the Coulomb modification of straight-line trajectories. In our finite-range Glauber model (FRGM) calculations we have used the nucleon-nucleon (NN) cross sections directly from Ref. [10]. Further details of the calculations can be found in Ref. [11]. At high projectile energies, in the zero-range limit the FRGM reduces to ZRG, as expected.

The predictions based on the BHF approach have been successfully applied [12,13] to study the rich variety of nucleon scattering data over a wide energy region. The additional important input for BHF calculations is the internucleon potential. We have used the old Hamada-Johnston (HJ) [14], Urbana v-14 [15], and the Argonne v-18 [16] internucleon potentials to calculate the microscopic proton-nucleus optical potential. We have not adjusted any parameters of the potentials. It is important to note that we have used the full potential, including spin orbit, in contrast with Ref. [1], where only the central part of the calculated potential was used. Further, we have checked that the inclusion of the spin-orbit potential has a negligible

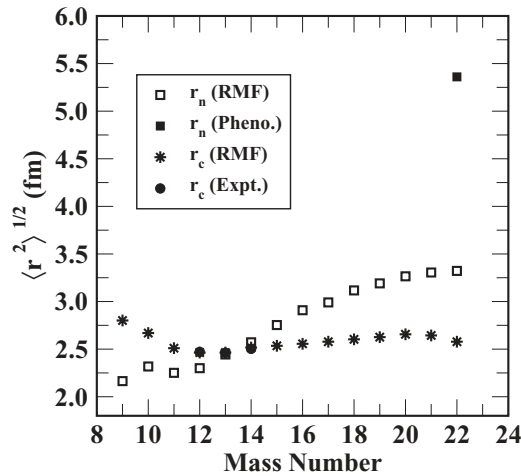


FIG. 1. Calculated (RMF) neutron ( $r_n$ ) and the charge ( $r_c$ ) rms radii. The experimental [7] values of  $r_c$  (wherever available) are shown. The value of  $r_n$  for  $^{22}\text{C}$  obtained with the phenomenological density [8] is also presented.

effect on the predictions of the reaction cross section. It is to be noted that there are no free parameters in our calculations, therefore, the reaction cross sections quoted in this Rapid Communication are our predictions.

The results are shown in Fig. 3. The figure reveals that the results of all three (HJ, v-14, and v-18) internucleon potentials employed in BHF are very close to each other and qualitatively similar to that of FRGM. It is indeed satisfying to note that both the Glauber model and the corresponding BHF predictions are in close agreement with each other. These results successfully reproduce the experimental data except for  $^{22}\text{C}$ , where the calculation underestimates the reaction cross section. To reproduce this enhancement we require an extended neutron distribution for  $^{22}\text{C}$ . For this purpose,  $^{22}\text{C}$  is regarded as  $^{20}\text{C}$  plus  $2n$ . To generate the core ( $^{20}\text{C}$ ) and the  $2n$  tail, we

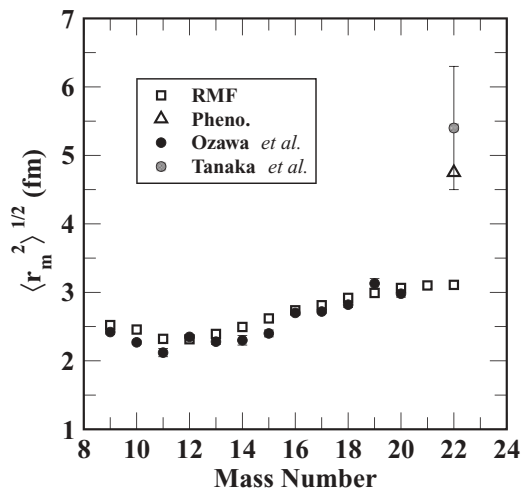


FIG. 2. Calculated (RMF) rms matter radii  $r_m$ . The values denoted by Ozawa *et al.* and Tanaka *et al.* are taken from Refs. [9] and [1], respectively. “Pheno.” corresponds to the value obtained by using the prescription of Ref. [8] for the extended neutron density distribution.

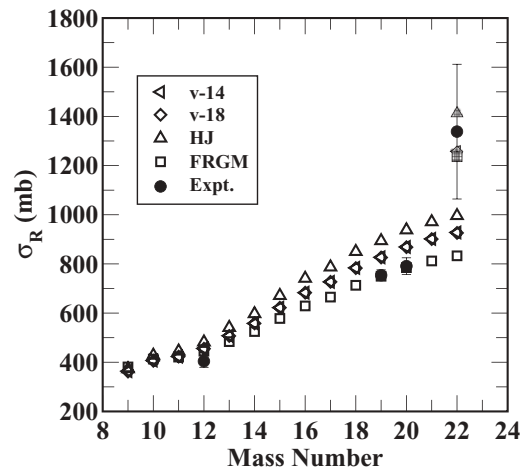


FIG. 3. The calculated reaction cross sections for 40-A MeV carbon isotopes incident on the proton target. Various abbreviations are self-explanatory and are also stated in the text.

follow the prescription proposed in our earlier work [8]. This requires the charge radius of  $^{20}\text{C}$  (taken from RMF) and the single neutron separation energy  $S_n$  of  $^{22}\text{C}$ , taken to be  $S_{2n}/2$  (210 keV) [3]. The extended neutron density distribution for  $^{22}\text{C}$  is shown in Fig. 4 along with that of  $^{20}\text{C}$  and the  $2n$  tail. The density distribution used by Tanaka *et al.* [1] is also shown in the same figure.

The calculated reaction cross sections (also shown in Fig. 3 by the corresponding hatched symbols) with this new input density for  $^{22}\text{C}$  now agree well with the experiment. This indicates that for  $^{22}\text{C}$  only the use of the extended neutron density distribution gives a reaction cross section that is in agreement with the experimental data, indicating the  $2n$ -halo structure in  $^{22}\text{C}$ .

It is desirable to use the present analysis for the description of the additional experimental observables to confirm the

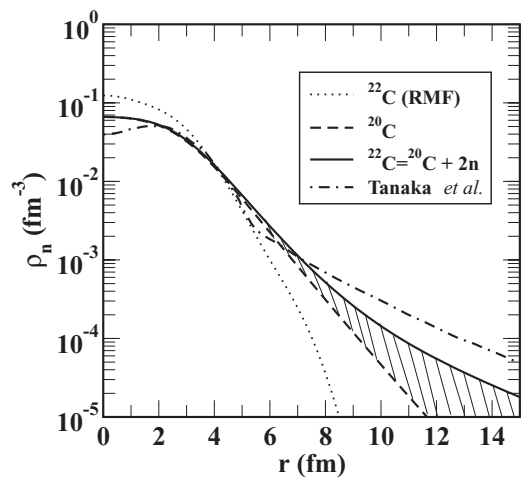


FIG. 4. The calculated neutron density distributions. The  $2n$  halo is shown by hatched lines. The corresponding distribution of Tanaka *et al.* [1] is also shown.

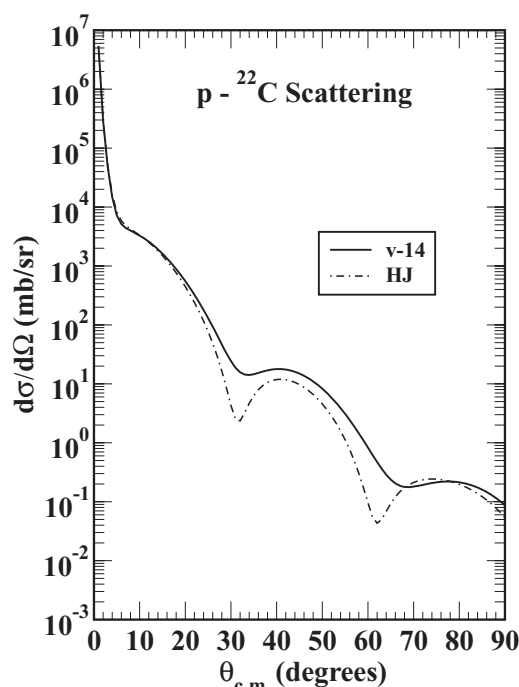


FIG. 5. The calculated differential cross sections for 40-A MeV  $^{22}\text{C}$  incident on a hydrogen target.

validity of the present approach. Unfortunately, data such as differential cross sections are not available for such systems. Therefore, as an illustration, we discuss the corresponding calculated differential cross sections for  $^{22}\text{C}$ . It is interesting to note that the BHF and FRGM results are very similar. However, there are minor differences at a finer level at higher angles ( $>20^\circ$ ). Specifically, the v-18 and v-14 results lie almost on

the top of each other, while HJ and FRGM results are almost identical. The HJ (hard core) and so also FRGM yields a slightly lower first minimum and its position shifts slightly toward a lower (higher) angle for HJ (FRGM). Therefore, only the results for v-14 and HJ are presented in Fig. 5.

In summary, the recently measured [1] reaction cross sections for the neutron-rich carbon isotopes ( $^{19}\text{C}$ ,  $^{20}\text{C}$ , and  $^{22}\text{C}$ ) on a proton target at 40 A MeV are analyzed using the finite-range Glauber model (FRGM) [11] and the microscopic optical potential calculated within the Brueckner-Hartree-Fock formalism (BHF). The NN cross sections are used in FRGM while the Hamada-Johnston (HJ), Urbana v-14, and the Argonne v-18 internucleon potentials are employed in BHF to calculate the microscopic optical potential. The nucleon density distributions calculated in the relativistic mean-field (RMF) approach are used. The analysis reveals that the BHF results of all three internucleon potentials are very close to each other, and also agree with the corresponding results of the FRGM. The calculations reproduce the experiment well, while for  $^{22}\text{C}$  the extended neutron density distribution is required to reproduce the observed enhanced cross section, indicating a halo structure for  $^{22}\text{C}$ , thus supporting the  $2n$ -halo structure for  $^{22}\text{C}$ . However, we feel that there is an urgent need to complement the present data with a differential elastic cross-section measurement to confirm the halo structure in  $^{22}\text{C}$ .

We are thankful to S. Kailas, S. H. Patil, Raghava Varma, and P. Schuck for their interest in this work. Partial financial support by the Department of Science and Technology (DST), Government of India, to A. Bhagwat and Y. K. Gambhir (Project No. SR/S2/HEP-034/2009) is gratefully acknowledged.

- 
- [1] K. Tanaka *et al.*, *Phys. Rev. Lett.* **104**, 062701 (2010).  
 [2] I. Tanihata *et al.*, *Phys. Rev. Lett.* **55**, 2676 (1985); *Phys. Lett. B* **206**, 592 (1988).  
 [3] A. H. Wapstra, G. Audi, and C. Thibault, *Nucl. Phys. A* **729**, 129 (2003).  
 [4] Y. K. Gambhir, P. Ring, and A. Thimet, *Ann. Phys. (NY)* **198**, 132 (1990).  
 [5] P. Ring, *Prog. Part. Nucl. Phys.* **37**, 193 (1996), and references therein.  
 [6] G. A. Lalazissis, J. König, and P. Ring, *Phys. Rev. C* **55**, 540 (1997).  
 [7] I. Angeli, *At. Data Nucl. Data Tables* **87**, 185 (2004).  
 [8] A. Bhagwat, Y. K. Gambhir, and S. H. Patil, *Eur. Phys. J. A* **8**, 511 (2000), and references therein.  
 [9] A. Ozawa *et al.*, *Nucl. Phys. A* **691**, 599 (2001).  
 [10] S. K. Charagi and S. K. Gupta, *Phys. Rev. C* **41**, 1610 (1990).  
 [11] A. Bhagwat and Y. K. Gambhir, *J. Phys. G* **36**, 025105 (2009), and references therein.  
 [12] W. Haider and Manjari Sharma, *Int. J. Mod. Phys. E* **19**, 465 (2010), and references therein.  
 [13] A. Öhrn *et al.*, *Phys. Rev. C* **77**, 024605 (2008).  
 [14] T. Hamada and I. D. Johnston, *Nucl. Phys.* **34**, 382 (1962).  
 [15] L. E. Lagaris and V. Pandhripande, *Nucl. Phys. A* **359**, 331 (1981).  
 [16] R. B. Wiringa, V. G. J. Stoks, and R. Schiavilla, *Phys. Rev. C* **51**, 38 (1995).